Supporting Information

Raising the CO_x Methanation Activity of a Ru/γ-Al_2O_3 Catalyst by Activated Modification of Metal-Support Interactions

Shilong Chen[1], Ali M. Abdel-Mageed[1], Michael Dyballa[2], Magdalena Parlinska-Wojtan[3], Joachim Bansmann[1], Simone Pollastri[4], Luca Olivi[5], Giuliana Aquilanti[5], and R. Jürgen Behm[1]**

[1] Institute of Surface Chemistry and Catalysis, Ulm University, D-89069 Ulm, Germany

[2] Institute of Technical Chemistry, Stuttgart University, D-70569 Stuttgart, Germany

[3] Institute of Nuclear Physics, Polish Academy of Sciences, PL-31-342 Krakow, Poland

[4] CERIC-ERIC, s.s. 14, km 163.5, I-34149 Trieste, Basovizza, Italy

[5] Elettra-Sincrotrone Trieste, s.s. 14, km 163.5, I-34149 Trieste, Basovizza, Italy

Table of Contents

1. Experimental section

Catalyst synthesis. 2.3 wt.% Ru/γ-Al_2O_3 catalyst was synthesized by an incipient wetness impregnation method, using commercial γ-Al_2O_3 from Johnson Matthey as support. This reproducibly resulted in highly dispersed and uniformly distributed Ru NPs. For impregnation with Ru, 189.9 mg of the Ru precursor ($RuCl_3$ hydrate, Sigma-Aldrich) was dissolved in 4.74 ml of Millipore water before adding 3 g of the support material (as received) under continuous stirring (250 rpm) for 1 h.

Catalytic measurements. The kinetic experiments were performed in a fixed-bed quartz tube micro-reactor (with 6 and 4 mm outer and inner diameter, respectively) at atmospheric pressure under a continuous flow of H_2-rich and CO_2-rich reformate gases either in the absence of CO (CO_2-ref: 15.5% CO_2, 80.9% H_2, N_2 balance) or in the presence of CO (SR-ref 6000: 0.6% CO, 15.5% CO_2, 80.9% H_2, N_2 balance), with a total gas flow of 41.6 Nml min^{-1} in all measurements. For comparison, selected measurements were performed in CO_2-free reformate (ID-ref 6000: 0.6% CO, 80.9% H_2, N_2 balance). For the kinetic measurements at 190°C the catalysts were diluted with varying amounts of catalytically inactive and thermally stable α-Al_2O_3 powder (calcined at 900 °C for 24h) to ensure differential reaction conditions (conversion < 20%). In total, about 200 mg of the diluted catalyst was used, resulting in a catalyst bed length of ~1.2 cm. This ensures a fixed space velocity in all experiments (28000 h^{-1}). After calcination (in 10% O_2 / N_2 at 150°C for 30 min) and subsequent ramping up of the temperature to 190°C in the respective reaction gas, the activity of the catalyst was evaluated in three subsequent phase: 1) over 1000 min on stream at 190°C (190°C-1 phase), 2) during a temperature programmed reaction sequence (TPR sequence): including 6 temperature steps (210, 230, 250, 270, 300, and 350°C), where each temperature was kept for 3 hour, 3) cooling down to 190°C and keeping that temperature for 1000 min (190°C-2

phase). The influent and effluent gases were analyzed by online gas chromatography with a CO detection limit of ca. 5 ppm (DANI 86.10), using thermal conductivity detectors (H_2 used as carrier gas) and a standard test gas mixture for calibration.

Reaction in CO_2-ref reformate gases. The Ru-mass-normalized reaction rate for CO_2 methanation ($CO_2 + 4H_2 \rightarrow CH_4 + 2H_2O$) was calculated from the CO_2 conversion (X_{CO2}) under differential reaction conditions ($X_{CO2} < 20\%$), the molar flow rate of CO_2 into the reactor ($n_{CO2,in}$), and the absolute mass of Ru metal (m_{Ru}) according to eq. 1. The Ru-mass-normalized CH_4 formation rate, in contrast, was calculated from the effluent molar flow rate of the CH_4 formed ($n_{CH4,out}$), which was produced from CO_2 (eq. 2). From these Ru-mass-normalized reaction rates, the turnover frequencies (TOFs) were calculated using the molar mass of Ru (M_{Ru}) and the Ru dispersion (D_{Ru}) obtained from TEM imaging according to eq. 3. The selectivity for CO_2 methanation ($S_{CH4(CO2)}$) with respect to reverse water-gas shift reaction (RWGS) is given by the ratio of the CO_2 methanation rate compared to that of the overall CO_2 conversion (methanation and RWGS, see eq. 4).

$$R_{CO_2} = \frac{X_{CO_2} \times n_{CO_2,in}}{m_{Ru}} \quad (1)$$

$$R_{CH_4} = \frac{n_{CH_4,out}}{m_{Ru}} \quad (2)$$

$$TOF = \frac{R_{CH_4} \times M_{Ru}}{D_{Ru}} \quad (3)$$

$$S_{CH_4(CO_2)} = \frac{R_{CH_4}}{R_{CO_2}} = \frac{R_{CH_4}}{R_{CH_4} + R_{CO}} \quad (4)$$

Reaction in SR-ref 6000 or ID-ref 6000 reformate gases. The Ru-mass-normalized reaction rate for CO methanation ($CO + 3H_2 \rightarrow CH_4 + H_2O$) was calculated from the CO conversion (X_{CO}) under differential reaction conditions ($X_{CO} < 20\%$), the molar flow rate of CO into the reactor ($n_{CO,in}$),

and the absolute mass of Ru metal (m_{Ru}) according to eq. 5. The Ru-mass-normalized CH_4 formation rate, in contrast, was calculated from the effluent molar flow rate of the CH_4 formed ($n_{CH4,out}$), which was produced from both CO and CO_2 (eq. 6). From these Ru-mass-normalized reaction rates, the turnover frequencies (TOFs) were calculated using the molar mass of Ru (M_{Ru}) and the Ru dispersion (D_{Ru}) obtained from TEM imaging according to eq. 7. The selectivity for CO methanation ($S_{CH4(CO)}$) with respect to CO_2 methanation is given by the ratio of the CO methanation rate compared to that of the overall methane formation (from CO and CO_2, see eq. 8).

$$R_{\mathrm{CO}} = \frac{\mathrm{X_{CO}} \times \mathrm{n_{CO,in}}}{\mathrm{m_{Ru}}} \quad (5)$$

$$R_{\mathrm{CH_4}} = \frac{\mathrm{n_{CH_4,out}}}{\mathrm{m_{Ru}}} \quad (6)$$

$$\mathrm{TOF} = \frac{R_{\mathrm{CH_4}} \times \mathrm{M_{Ru}}}{\mathrm{D_{Ru}}} \quad (7)$$

$$S_{CH4(CO)} = \frac{R_{\mathrm{CO}}}{R_{\mathrm{CH_4}}} = \frac{R_{\mathrm{CO}}}{R_{\mathrm{CO}} + R_{\mathrm{CO_2}}} \quad (8)$$

Catalyst characterization.

Ru loading and surface area of the catalysts: The Ru loadings of the Ru/Al_2O_3 catalyst was determined by inductively coupled plasma optical emission spectroscopy (ICP-OES), indicating similar Ru loadings of 2.3 wt.% for Ru/Al_2O_3. The specific surface area was measured by N_2 adsorption (BET), yielding rather similar values of ~130 m^2g^{-1} for Ru/Al_2O_3.

Electron Microscopy (EM): The Ru particle shape and size of both Ru/γ-Al_2O_3-ISO and Ru/γ-Al_2O_3-TPR catalysts were determined from bright field transmission electron microscopy (TEM) and high-angle annular dark-field scanning transmission electron microscopy (HADDF-STEM) images, which were performed on a Cs-corrected FEI Titan electron microscope operated at 300

keV. For detailed information on the Ru particle size (volume-area mean diameter and size distribution) and Ru particle shape (hemispherical and flat), at least 600 particles were evaluated for each sample. Assuming hemispherical Ru nanoparticles and a surface density of 1.5×10^{15} Ru atoms cm^{-2}, the Ru dispersion was calculated from the volume-area mean diameter.

Dispersion of Ru nanoparticles: Calculation from TEM results: With the known diameter (d_i) of the individual of Ru nanoparticles (n_i), as measured by TEM, the volume-area mean diameter (d_{VA}) was calculated according to equation (9). From this relation one can easily calculate the Ru metal dispersion (D_{Ru}), which is defined by the ratio of surface atoms to the total number of atoms in the hemispherical metal particle (V_{Ru} = volume Ru atom, a_{Ru} = surface area Ru atom) as shown in equation (10).

$$d_{VA} = \frac{\sum_i n_i d_i^3}{\sum_i n_i d_i^2} \qquad (9)$$

$$D_{Ru} = 6 \frac{V_{Ru}/a_{Ru}}{d_{VA}} \qquad (10)$$

X-ray diffraction (XRD): XRD measurements of the Ru catalysts after reaction at 190°C-1 and 190°C-2 in SR-ref 6000 reformate were performed on a Siemens D5000 diffractometer, using Cu K_α radiation ($\lambda = 0.154$ nm).

X-ray photoelectron spectroscopy (XPS): XP spectra were recorded on a PHI 5800 ESCA system (Physical Electronics), using monochromatized Al K_α radiation (1486 eV). The pass energy for survey spectra was 93.9 eV, for detail spectra we used 29.35 eV. Spectra of the Ru catalysts were recorded after reaction at 190°C-1 and 190°C-2. The binding energies (BEs) of all spectra were calibrated with respect to the C (1s) peak of ubiquitous carbon, which was fixed at a binding energy of 284.8 eV. The deconvolution of XP spectra was performed using a public XPS peak fitting program (XPSPEAK4.1).

Solid-state nuclear magnetic resonance (NMR): Solid state NMR spectroscopy on aluminum was performed on a Bruker Avance III 400WB spectrometer at a resonance frequency of 104.3 MHz applying spinning around the magic angle (MAS) at 8 kHz. The ^{27}Al MAS NMR spectra were recorded by summarizing 3200 scans, performed with repetition time of 0.5 s, and each one recorded after $\pi/12$ pulse direct excitation. Prior to measurements, the samples were fully hydrated for 12 h in a desiccator over a saturated aqueous solution of $Ca(NO_3)_2$.

***In situ* diffuse reflectance FTIR spectroscopy (DRIFTS).** *In situ* DRIFTS measurements were performed on a Nicolet iS-50 FTIR spectrometer, equipped with an *in-situ* DRIFTS reaction cell (HV-DR2, Harrick Scientific). The DRIFTS spectra were measured with a resolution of 4 cm^{-1}, using a MCT narrow band detector. The catalyst was calcined and activated in the same way as in the kinetic measurements. The reaction of the Ru catalysts was followed in both SR-ref 6000 and ID-ref 6000 gas reformate during reaction at 190°C (190°C-1 phase) for 1000 min, during the subsequent TPR sequence, and finally during the 190°C-2 phase for 600 min, while continuously recording DRIFT spectra (400 scans recorded per spectrum for each 15 min). The intensities of adsorbed species were evaluated in Kubelka−Munk units (KMU), derived from the reflectance, R_v, via the equation $KMU_v = (1 - R_v)^2/2R_v$, which are generally proportional to the adsorbate concentration.[1] The peak-fitting of DRIFT spectra were processed with the peak deconvolution function of Nicolet's OMNIC Spectra Software.[2]

After reaction, the spent catalysts were purged in N_2 for 1000 min at 190°C to remove the adsorbed CO, weakly bound hydrocarbons and H_2O / OH species on the catalysts. Low-temperature CO adsorption experiments were subsequently performed on these catalysts in a CO flow (1% CO / N_2) at 30°C for 1h. Subsequently catalyst and reaction cell were purged with N_2 to remove the gas-phase CO signal.

Pyrrole Titration Measurement. First, the spent catalysts were purged with N_2 at 190 °C for 1000 min to desorb stable adsorbates. Subsequently they were cooled down in N_2 to 30°C. Then a pyrrole / N_2 mixture, which was prepared by bubbling pure N_2 through a bath containing pure pyrrole at 6°C (0.3 vol.% gas phase concentration), was passed over the catalyst bed at 30 °C for 60 min, while recording *in situ* DRIFT spectra. Afterwards, the catalysts were purged in N_2 for 10 min to remove the gas phase pyrrole and weakly adsorbed pyrrole species, followed by a temperature programmed desorption (TPD) scan (in N_2, from 30 to 450°C, heating rate 10°C min^{-1}). Finally, the temperature was held for 15 min at 450°C to complete desorption. The concentration of pyrrole in the effluent gases during the pyrrole desorption measurements was analyzed by IR transmission measurements in a Bruker Alpha FTIR spectrometer (Bruker Optics Inc., Ettlingen, Germany), using a substrate-integrated hollow waveguide (iHWG) for enhanced sensitivity.[3] All IR spectra were recorded in the spectral range of 700 – 4000 cm^{-1} at a resolution of 4 cm^{-1}. To remove contributions from pyrrole adsorption on the reactor walls etc., we determined desorption from an empty reactor after a similar adsorption procedure and subtracted this from the desorption rates measured for the different catalysts. In a similar way we also verified that the α-Al_2O_3 used for catalyst dilution is not active for pyrrole adsorption under these conditions.

***Operando* X-ray Absorption Spectroscopy (XAS) Measurements.** Time-resolved *operando* XANES and EXAFS measurements were performed in transmission in a continuous mode at the Ru K-edge (22117 eV) at the P65 beamline of the PETRA-III extension (DESY) and at the XAFS beamline of the Elettra Synchrotron, using a Si(311) double crystal monochromator.[4] The data acquisition took 3-5 min per spectrum. For the measurements we employed a specially designed reaction cell made of brass, which was previously used in similar XAS measurements.[5] The reaction kinetics during XAS measurement were monitored by transmission infrared spectrometry,

using an FTIR spectrometer (Alpha Bruker Optics Inc.) coupled with an substrate-integrated hollow wave guide (iHWG) for higher sensitivity.[3] For the 190°C-1 phase, the shorter reaction time in the *operando* XAS measurements (140 min) was still by far enough to reach steady-state conditions. During the TPR sequence, the measurements were performed over 60 min at each temperature, as compared to 3 h in the kinetic measurements, which may not fully suffice for reaching steady state at the high temperatures. During the 190°C-2 phase, the XAS measurements were performed over 250 min on stream, where according to the kinetic measurements the catalyst is already very close to steady-state conditions. Despite the higher space velocity in the XAS measurements, which resulted in different reaction rates compared to the kinetic measurements in the fixed-bed micro-reactor (at 190°C), the trend of an enhanced activity after the TPR sequence agrees well with the corresponding micro-reactor results (for kinetic data during *operando* XAS measurements, see Figure S17). A Ru foil, a pellet of Ru(IV) oxide and $RuCl_3$, which were measured in transmission mode, were used as reference materials for the data evaluation. Background removal and spectra normalization as well as the linear combination analysis (LCA) of the XANES spectra were performed using the Athena software from the IFEFFIT program package.[6;7] The data reduction and subsequent fits of EXAFS spectra were carried out using the XDAP software package with standard procedures described elsewhere.[8;9] Theoretical references were calculated by FEFF 8.0 and calibrated with experimental references of Ru foil and RuO_2 powder.[10;11] The EXAFS data were evaluated in the R-space (R: 0.0 − 4.3 Å), using the k-range from 3.2 to 11.8 $Å^{-1}$. In the EXAFS data fit, we allowed the coordination number (CN), the parameter σ in the Debye-Waller factor (DWF), the Ru-Ru bond length (R), and the energy shift (E_0) to change freely (see Table S3). Note that the Ru-O-Ru scattering contribution was neglected in the EXAFS analysis due to negligible contribution from oxidic Ru species during reaction.

H-D exchange reaction measurement

H-D exchange measurements were performed in a fixed-bed micro-reactor using online mass spectrometry (MS, OMG700, Pfeiffer) About 200 mg of the diluted catalyst (1:19 with α-Al_2O_3) were used. The spent catalysts include Ru/γ-Al_2O_3-ISO (after the first isothermal reaction at 190°C for 1000 min (190°C-1 phase)) and Ru//γ-Al_2O_3-TPR (after TPR sequence and second isothermal reaction at 190°C (190°C-2 phase)). Afterwards, the reacted catalyst was purged with N_2 at 190 °C for 1000 min, to desorb stable adsorbates. During H-D exchange reaction, the feed gas consists of 10% deuterium (D_2), 10% H_2 with N_2 as balance gas. The total flow rate was kept at 30 ml min^{-1}.

2. Catalytic performance of the Ru-based catalysts

Table S1 Comparison of catalytic performances of Ru-based catalysts in the selective CO methanation.

Catalyst	Ru loading (wt.%)	Ru NP size	Reformate gases (%)				Space velocity ($ml\ h^{-1}\ g^{-1}$)	Temperature (°C)	CO methanation rate ($\mu mol_{CH4}\ g_{Ru}^{-1}\ s^{-1}$)	S_{CO} (%)	Notes
			CO	CO_2	H_2	N_2 /He					
Ru/γ-Al_2O_3-ISO	2.3	1.5	0.6	15.5	80.9	3	12480	190	5	100	This work
Ru/γ-Al_2O_3-TPR	2.3	1.8	0.6	15.5	80.9	3	12480	190	25	100	This work
Ru/TiO_2	2.2	1.5	0.6	15.5	80.9	3	12480	190	24.6	100	Ref. [12]
Ru/zeolite	2.2	1.1	0.6	15.5	80.9	3	12480	190	39	100	Ref. [13]
Ru/γ-Al_2O_3	2.0	1.5	1	15	50	34	80000	215	0.56	~100	Ref. [14]
Ru/TiO_2	2.0	3.2	1	15	50	34	80000	215	1.89	~100	

3. Surface area, pore volume and pore size of the Ru/γ-Al_2O_3 catalysts

Table S2 BET specific surface area, pore volume and pore size of Ru/γ-Al_2O_3-ISO (after reaction in SR-ref 6000 reformate gas at the first 190°C for 1000 min) and Ru/γ-Al_2O_3-TPR (after subsequent TPR sequence and second 190°C phase for 1000 min).

Catalyst	Surface area (m^2 g^{-1})	Pore volume (cm^3 g^{-1})	Average pore size (nm)
Ru/γ-Al_2O_3-ISO	123	0.91	21.70
Ru/γ-Al_2O_3-TPR	131	0.92	22.13

4. EXAFS structural parameters

Table S3 Structural parameters extracted from the evaluation of EXAFS spectra collected on the Ru/Al_2O_3 catalyst during reaction in SR-ref 6000 reformate.

Temperature and Time	Scatterer	CN ± 0.5	σ^2 ($Å^2$) ± 0.0004	R (Å) ± 0.02	E_0 (eV)
150°C after calcination	Ru-O Ru-Ru	5.0 1.9	0.018 ± 0.01 0.011 ± 0.005	2.2 ± 0.1 2.7 ± 0.1	-19 ± 6 17 ± 6
190°C-1 /5 min	Ru-Ru	3.2	0.0028 ± 0.001	2.67	17 ± 6
190°C-1 /8 min	Ru-Ru	4.5	0.0042	2.67	8 ± 3
190°C-1 /30 min	Ru-Ru	5.7	0.0043	2.67	7 ± 2
190°C-1 /55 min	Ru-Ru	5.7	0.0041	2.67	9 ± 3
190°C-1 /79min	Ru-Ru	5.3	0.0043	2.67	4 ± 2
190°C-1 /115 min	Ru-Ru	6.0	0.0045	2.67	8 ± 3
210°C /60 min	Ru-Ru	5.0	0.0043	2.67	6 ± 2
230°C /60 min	Ru-Ru	5.0	0.0043	2.68	10 ± 3
250°C /60 min	Ru-Ru	5.5	0.0043	2.66	10 ± 3
270°C /60 min	Ru-Ru	5.3	0.0043	2.65	9 ± 3
300°C /60 min	Ru-Ru	5.4	0.0043	2.64	7 ± 2
350°C /60 min	Ru-Ru	4.8	0.0043	2.64	9 ± 3
190°C-2 /5 min	Ru-Ru	5.6	0.0043	2.67	7 ± 3
190°C-2 /18 min	Ru-Ru	5.4	0.0042	2.67	9 ± 3
190°C-2 /51 min	Ru-Ru	5.8	0.0039	2.67	9 ± 3
190°C-2 /120 min	Ru-Ru	5.8	0.0040	2.67	7 ± 2
190°C-2 /185 min	Ru-Ru	5.6	0.0043	2.67	6 ± 2
190°C-2 /225 min	Ru-Ru	5.6	0.0043	2.67	6 ± 2
190°C-2 /265 min	Ru-Ru	5.8	0.0042	2.67	5 ± 2

CN: Ru-Ru and Ru-O first shell coordination number. σ^2: mean squared displacement, part of the Debye-Waller-Factor (DWF): $\exp(-2\sigma^2 k^2)$ with k being the wave vector. R: Ru-Ru or Ru-O bond distance. E_0: energy reference parameter. In these fits, the amplitude correction factor (S_0^2) was kept at a value between 0.85 and 1.0. Error bars given top row apply to values where no separate error bars are given.

5. CO methanation in ID-ref 6000

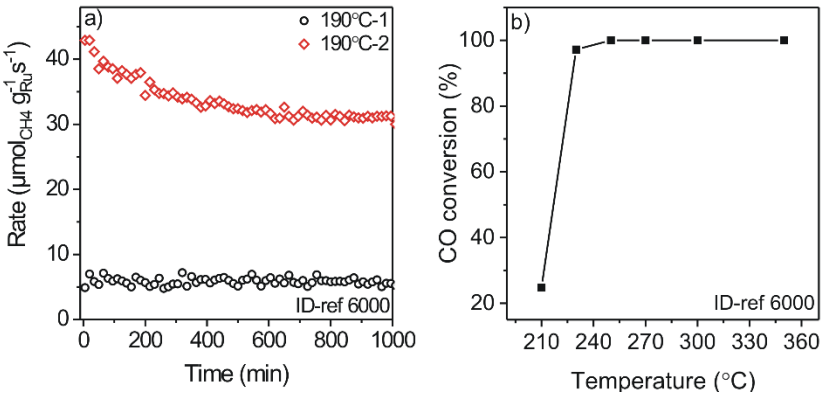

Figure S1 Temporal evolution of Ru-mass-normalized reaction rate (a) for CO methanation at 190°C and CO conversion during TPR treatment (b) in ID-ref 6000 reformate gas.

The Ru/γ-Al_2O_3 catalyst showed a stable reaction rate ~5.5 $\mu mol_{CH4}\ g_{Ru}^{-1}\ s^{-1}$ in the 190°C-1 reaction phase and reached a higher rate of ~42.9 $\mu mol_{CH4}\ g_{Ru}^{-1}\ s^{-1}$ after the TPR sequence, during the 190°C-2 reaction phase in the initial reaction time with a continuous deactivation after TPR treatment. This results in a steady-state rate of ~31.2 $\mu mol_{CH4}\ g_{Ru}^{-1}\ s^{-1}$ after reaction for 600 min, reflecting a ~5-fold higher rate than at 190°C-1.

6. Diffractograms of the Ru/γ-Al_2O_3 catalysts

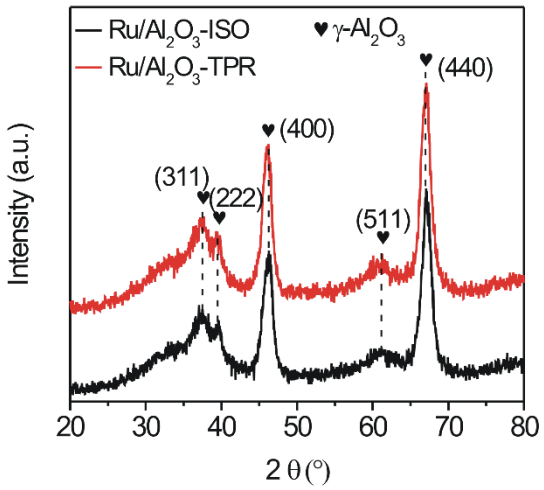

Figure S2 XRD diffractograms of the Ru/γ-Al_2O_3 catalysts.

7. ^{27}Al MAS NMR spectra of the Ru/γ-Al_2O_3 catalysts

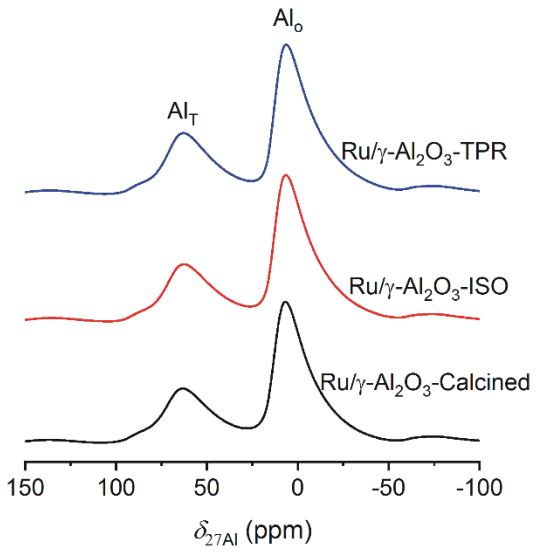

Figure S3 The ^{27}Al MAS NMR spectra of Ru/γ-Al_2O_3 after calcination, Ru/γ-Al_2O_3-TPR, and Ru/γ-Al_2O_3-ISO catalysts (from bottom to top).

The two peaks at 7 and 63 ppm are assigned to Al^{3+} ions in octahedral (A_o) and tetrahedral (A_t) coordination sites, respectively.

8. Additional HAADF-STEM and TEM images and Ru particle size distribution of the Ru/γ-Al_2O_3 catalysts

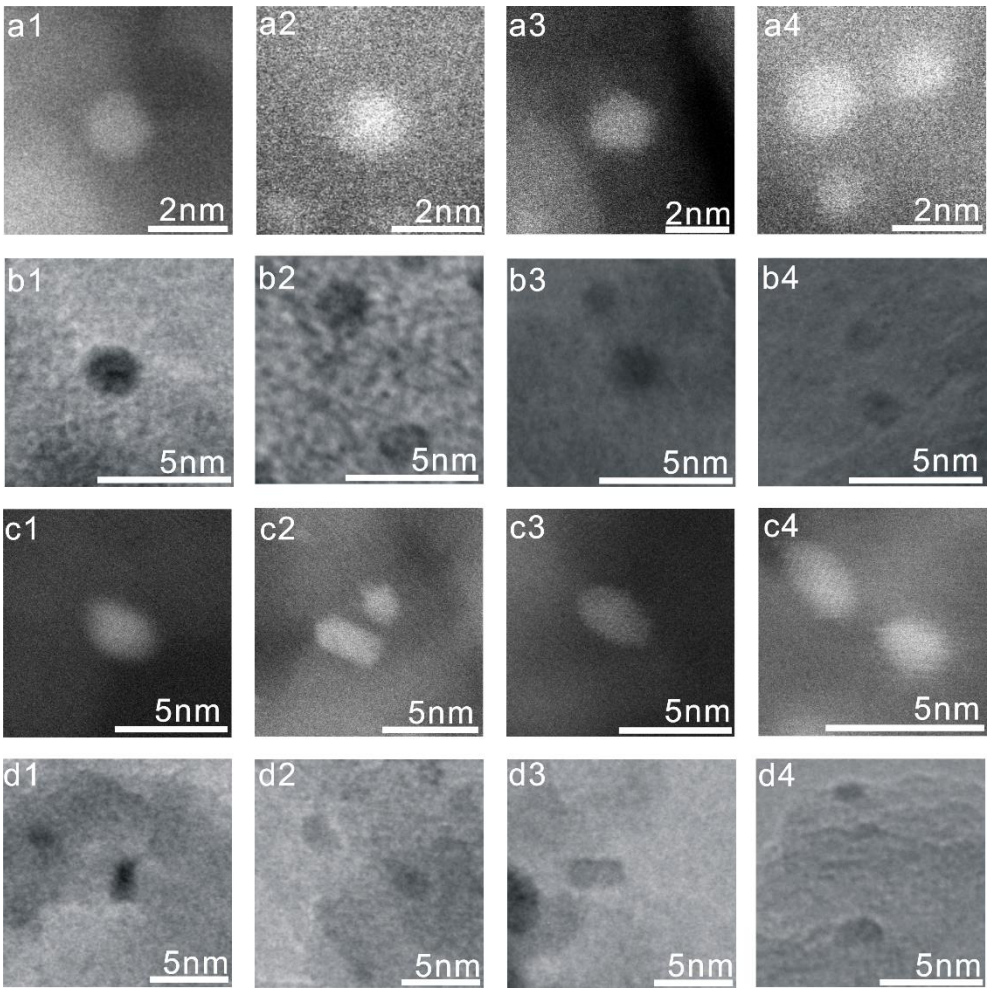

Figure S4 Additional HAADF-STEM and TEM images of the Ru/γ-Al_2O_3-ISO catalyst, after the first isothermal reaction (190°C-1) (a1-4 and b1-4), and of the Ru/γ-Al_2O_3-TPR catalyst, after the TPR sequence and the second isothermal reaction (190°C-2) (c1-4 and d1-4) in SR-ref 6000 reformate gas.

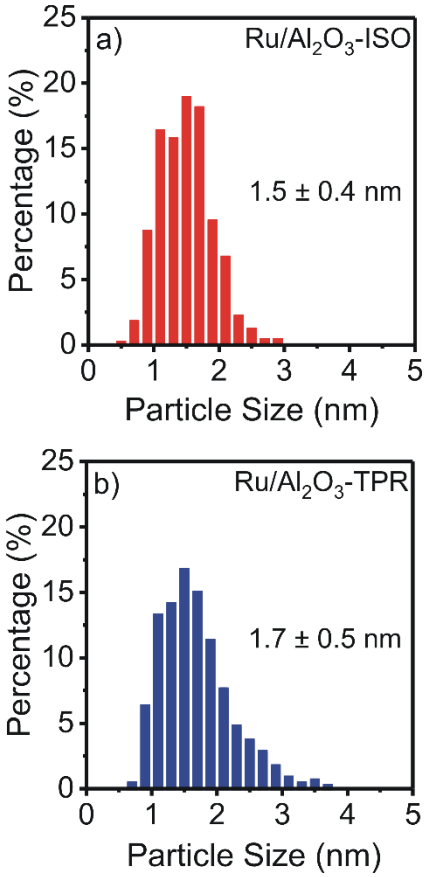

Figure S5 Ru particle size distributions of the Ru/γ-Al_2O_3-ISO catalyst after the first isothermal reaction (190°C-1) (a) and of the Ru/γ-Al_2O_3-TPR catalyst after the TPR sequence and the second isothermal reaction (190°C-2) (b) in CO_2-ref reformate gas.

9. Additional XAS spectra of the Ru/γ-Al_2O_3 catalysts

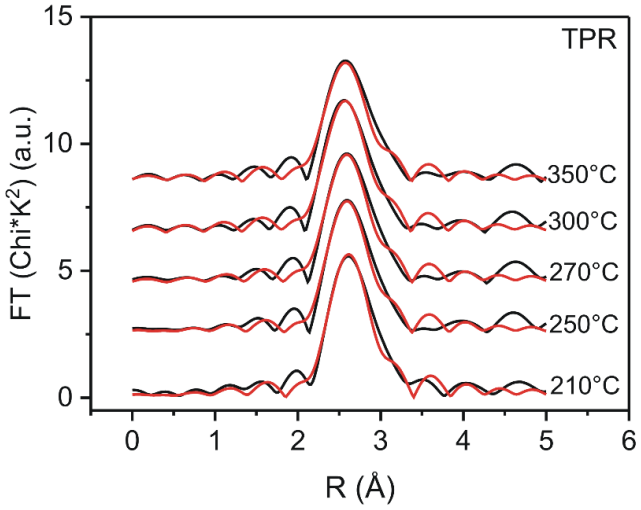

Figure S6 Fourier transformed EXAFS spectra in R-space recorded at the Ru K-edge at different reaction temperatures on the Ru/γ-Al_2O_3 catalyst in SR-ref 6000 at 190°C during the TPR sequence (black lines: measured EXAFS data, red lines: fit data.

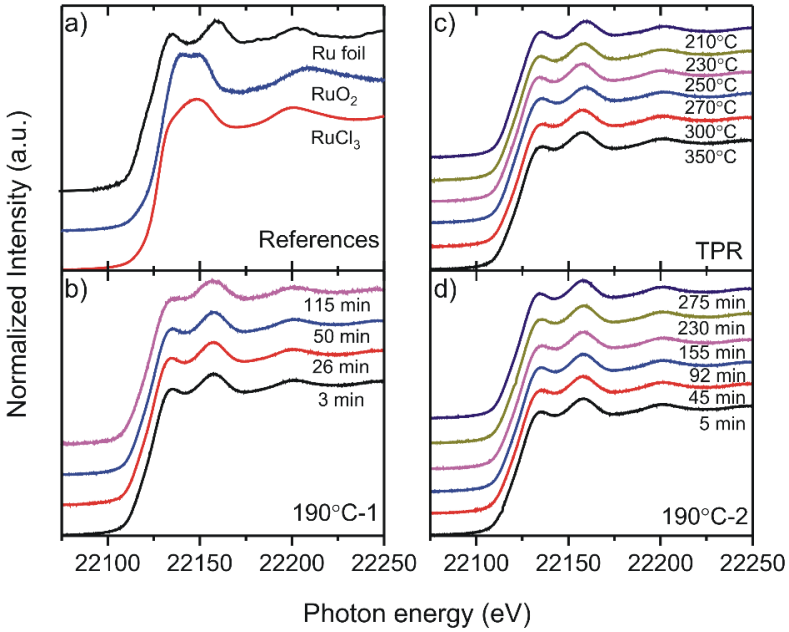

Figure S7 XANES spectra of references: Ru foil, RuO_2, $RuCl_3$ powder (a) and of the Ru/γ-Al_2O_3 catalyst during reaction in SR-ref 6000 reformate at 190°C (190°C-1) (b), during the TPR sequence (c), and during 190°C-2 (d) at different reaction times.

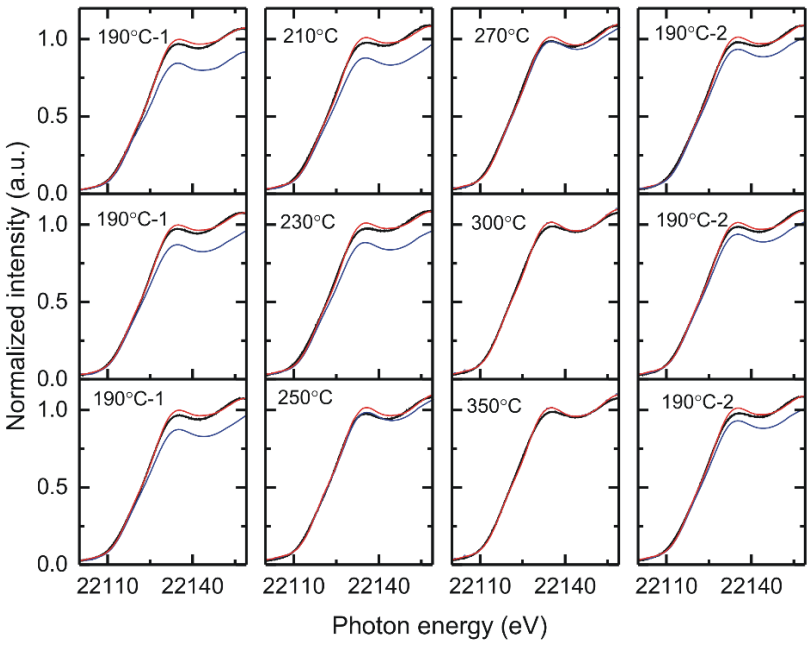

Figure S8 Linear combination analysis of selected Ru K-edge XANES spectra at different reaction times of Ru/γ-Al_2O_3 during reaction in SR-ref 6000 reformate gas. Black lines: original spectra, red lines: fit curves based on a linear combination of Ru references (Ru foil, RuO_2 and $RuCl_3$ powder), blue lines: metallic Ru species contribution.

10. Additional XPS spectra of the Ru/γ-Al_2O_3 catalysts

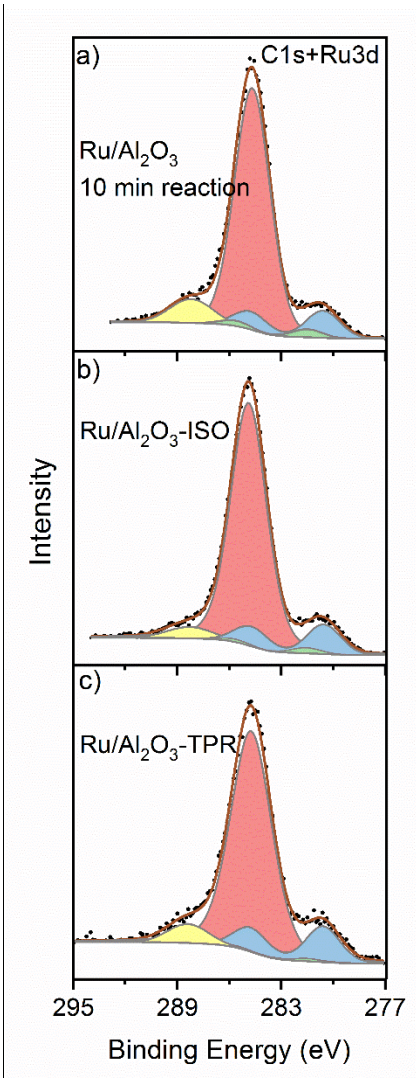

Figure S9 XP spectra of the Ru 3d / C 1s region of the Ru/γ-Al_2O_3 catalyst after 10 min reaction in the 190°C-1 phase (a), of the Ru/γ-Al_2O_3-ISO catalyst after reaction in the first isothermal reaction phase (190°C-1) (b), and the Ru/γ-Al_2O_3-TPR catalyst after the TPR sequence and subsequent isothermal reaction (190°C-2) (c) in SR-ref 6000 reformate gas. The different fit peaks refer to metallic Ru species: Ru $3d_{5/2}$: 280.6 eV and Ru $3d_{3/2}$: 284.7 eV (blue), oxidic Ru species: Ru $3d_{5/2}$: 281.5 eV and Ru $3d_{3/2}$: 285.6 eV (green), C 1s (ubiquitous carbon, red)); 284.8 eV, C 1s (formates, carboxylates, yellow): 288.5 eV.

The Ru 3d binding energies showed no shift / change after longer reaction (b) and after the temperature programmed reaction sequence (c). It should be noted that the BEs of oxidic

Ru are characteristic for Ru^{3+}/Ru^{4+} species in $RuCl_3$ and RuO_2 [15] and that the contributions from these species have a considerable error range. For the Ru/γ-Al_2O_3-TPR, the contribution from this species is at or below the level of significance.

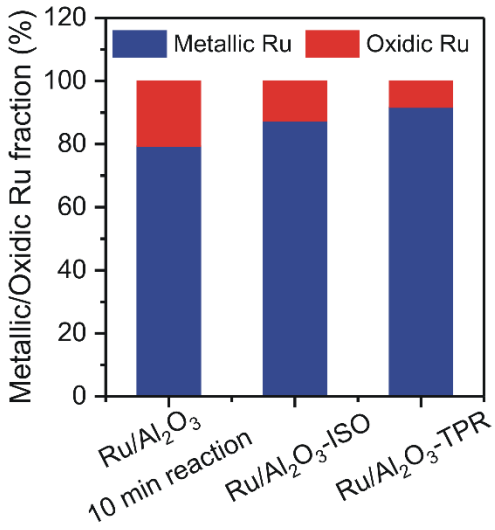

Figure S10 Contributions of metallic and oxidic Ru surface species of Ru/γ-Al_2O_3 after 10 min reaction in 190°C-1 phase, for the Ru/γ-Al_2O_3-ISO, and the Ru/γ-Al_2O_3-TPR catalyst after reaction in SR-ref 6000 reformate gas as derived from the XPS results in Figure S10.

11. Time-resolved *in situ* DRIFT spectra recorded during the TPR sequence

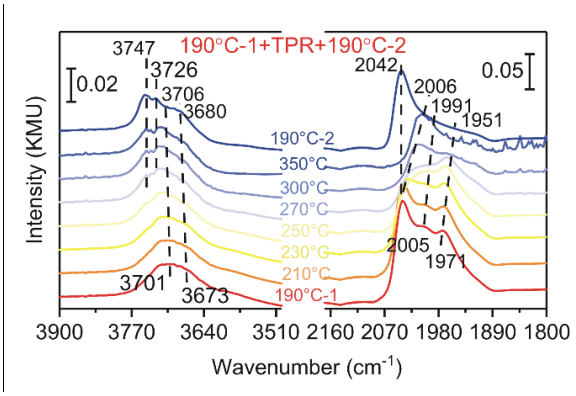

Figure S11 Time-resolved *in situ* DRIFT spectra of OH (in ID-ref 6000 reformate gas) and CO_{ad} regions (in SR-ref 6000 reformate gas) recorded during reaction at different temperatures as indicated in the figure. For comparison of CO_{ad} regions in SR-ref 6000 and ID-ref 6000 reformate gases see also Figure S10 below.

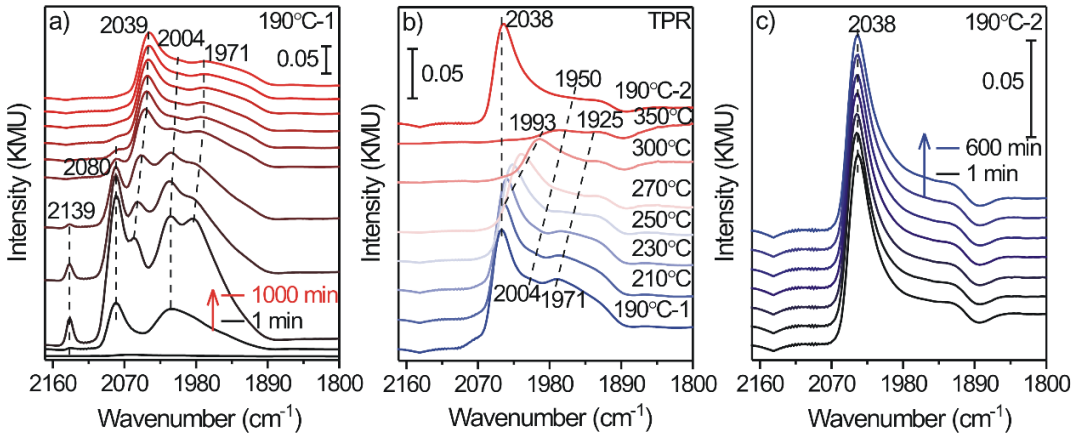

Figure S12 Time-resolved *in situ* DRIFT spectra of the CO region recorded in ID-ref 6000 reformate gas (a) at different times during reaction at 190°C-1 phase (after 1, 2, 5, 7, 10, 20, 60, 120, 360, 660, 1000 min), (b) at different temperatures during the TPR sequence, and c) at different times during reaction in the 190°C-2 phase (after 1, 60, 120, 240, 360, 480, 600 min).

12. Pyrrole titration´of basic surface sites

The DRIFTS measurements in Figure 6c in the main text manuscript show a broad absorption band around ~3480 - 3200 cm^{-1} for both Ru/γ-Al_2O_3 catalysts (Ru/γ-Al_2O_3-ISO and Ru/γ-Al_2O_3-TPR catalysts), which was assigned to the N-H stretch vibration of adsorbed pyrrole interacting with basic O^{2-} species on the support surface.[16] Bands at 3517, 3530 and 3542 cm^{-1} were assigned to the N-H stretch vibrations of gas phase pyrrole, while that at 3621 cm^{-1} is characteristic for surface hydroxyl groups interacting with pyrrole.[16;17] C-H stretch vibrations of gas phase pyrrole appear at 3063-3138 cm^{-1}.

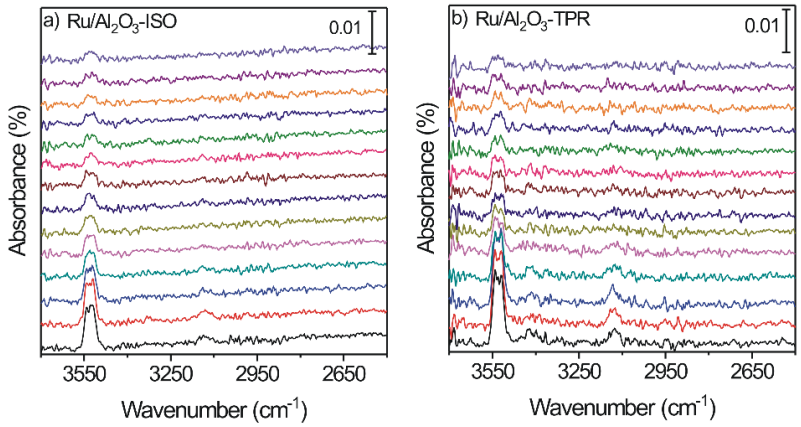

Figure S13 FTIR transmission spectra of the pyrrole gas phase (N-H stretching region) from the effluent gases during the TPD process for (a) Ru/γ-Al_2O_3-ISO and (b) Ru/γ-Al_2O_3-TPR catalysts, from bottom to top: 30, 67, 113, 158, 204, 250, 296, 345, 388, 433, 450, 450, 450, 450 °C.

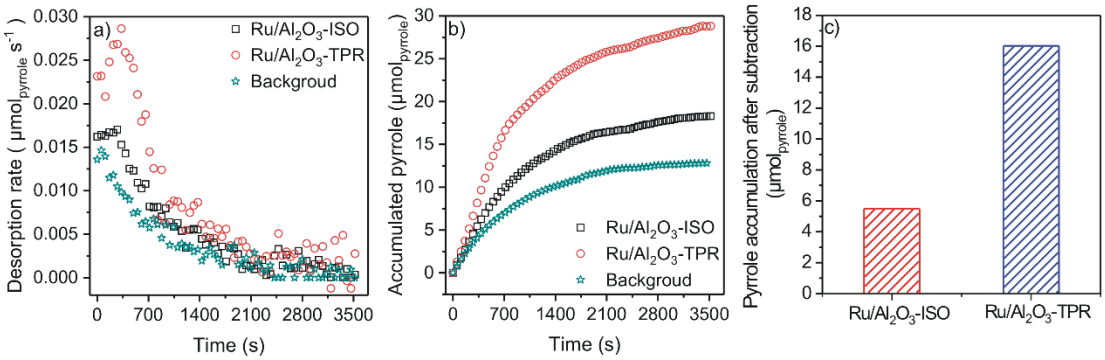

Figure S14 Pyrrole desorption rates from the three catalysts and from a background measurement (empty reactor) during temperature programmed desorption between 30°C and 450°C (10°C min^{-1}) (a), accumulated amount of desorbed pyrrole against time (b), and total amount of desorbed pyrrole after correction for background contributions (c). (The used catalyst mass was 7.27 mg for both Ru/γ-Al_2O_3-ISO and Ru/γ-Al_2O_3-TPR catalysts).

13. *In situ* DRIFT spectra of pure alumina support

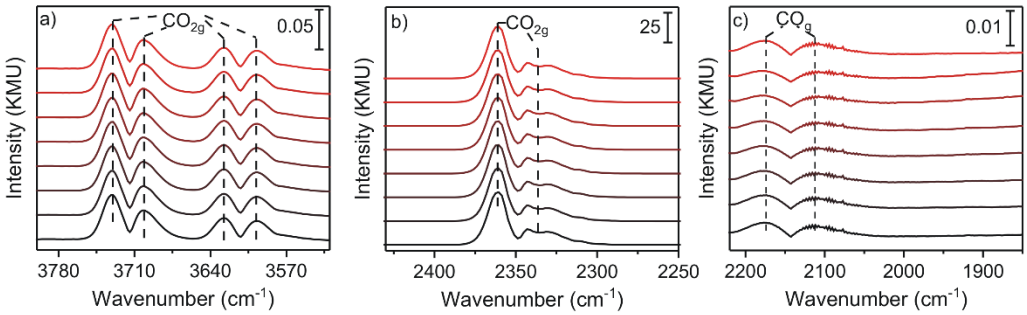

Figure S15 Different spectral regions of *in situ* DRIFT spectra of pure alumina support recorded in SR-ref 6000 reformate gas. (a) 3530-3800 cm^{-1} (CO_2 gas phase), (b) 2250-2430 cm^{-1} (CO_2 gas phase), and (c) 2220-1850 cm^{-1} (CO gas phase) (from bottom to top: 190°C-1, 210°C, 230°C, 250°C, 270°C, 300°C, 350°C, 190°C-2).

14. H/D exchange

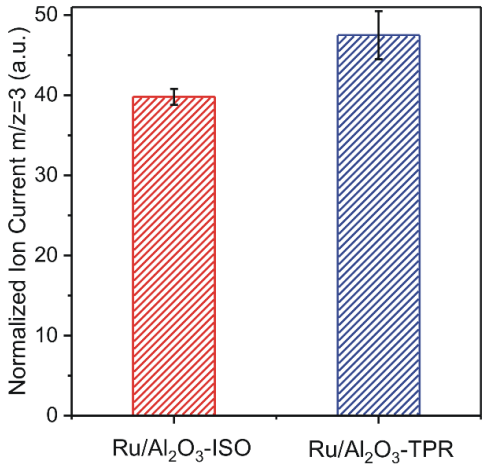

Figure S16 H/D exchange (m/z = 3, HD) in the reaction of H_2 with D_2 over Ru/γ-Al_2O_3-ISO and Ru/γ-Al_2O_3-ISO catalysts at 190°C.

The normalized ion current of m/z = 3 (HD) was calculated by the ion current of HD during H / D exchange measurement normalized by the ion current of HD during a bypass measurement (without passing through the catalyst bed).

15. Catalytic performance in the XAS reactor

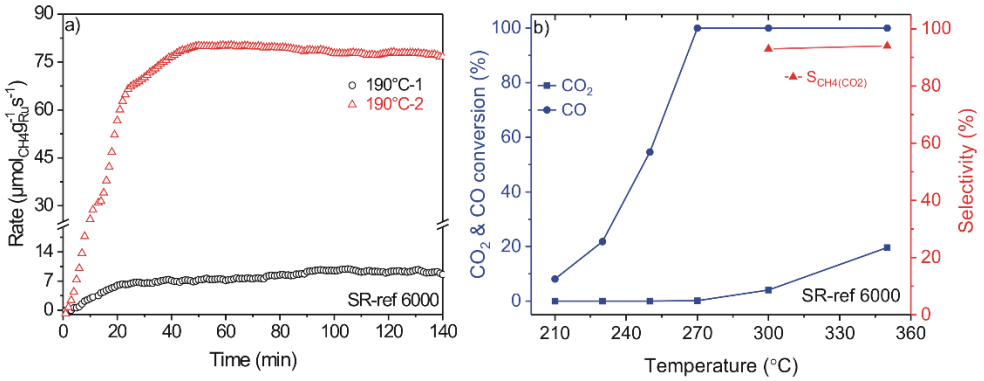

Figure S17 a) Temporal evolution of the Ru-mass-normalized reaction rate during CO methanation in SR-ref 6000 reformate gas during the first isothermal reaction (190°C-1) and second isothermal reaction after the TPR sequence (190°C-2). b) CO & CO_2 conversion and selectivity for CO_2 methanation ($S_{CH4(CO2)}$) with respect to the CO_2 consumption during reaction in SR-ref 6000 reformate in the temperature range of 210 to 350°C. The data were collected from the XAFS cell during the XAS measurements (catalyst mass: 25.6 mg Ru/γ-Al_2O_3 catalyst).

16. References

[1] J. Sirita, S. Phanichphant, F.C. Meunier, *Anal. Chem.* **2007,** *79,* 3912.

[2] S. Chen, L. Luo, Z. Jiang, W. Huang, *ACS Catal.* **2015,** *5,* 1653.

[3] V. Kokoric, D. Widmann, M. Wittmann, R.J. Behm, B. Mizaikoff, *Analyst* **2016,** *141,* 5990.

[4] A. Di Cicco, G. Aquilanti, M. Minicucci, E. Principi, N. Novello, A. Cognigni, L. Olivi, *J. Phys. :Conf. Series* **2009,** *190,* 012043-7.

[5] S. Chen, A.M. Abdel-Mageed, D. Li, J. Bansmann, S. Cisneros, J. Biskupek, W. Huang, R.J. Behm, *Angew. Chem. Int. Ed.* **2019,** *58,* 10732.

[6] M. Newville, *J. Synchrotron Rad.* **2001,** *8,* 322.

[7] B. Ravel, M.A.T.H. Newville, *J. Synchrotron Rad.* **2005,** *12,* 537.

[8] M. Vaarkamp, J.C. Linders, D.C. Koningsberger, *Physica B* **1995,** *208-209,* 159.

[9] S. Bordiga, E. Groppo, G. Agostino, J.A. van Bokhoven, C. Lamberti, *Chem. Rev.* **2015,** *113,* 1736.

[10] A.L. Ankudinov, B. Ravel, J.J. Rehr, S.D. Conradson, *Phys. Rev. B* **1998,** *58,* 7565.

[11] D.C. Koningsberger, B.L. Mojet, G.E. van Dorssen, D.E. Ramaker, *Top. Catal.* **2000,** *10,* 143.

[12] A.M. Abdel-Mageed, D. Widmann, S.E. Olesen, I. Chorkendorff, J. Biskupek, R.J. Behm, *ACS Catal.* **2015,** *5,* 6753.

[13] A.M. Abdel-Mageed, S. Eckle, H.-G. Anfang, R.J. Behm, *J. Catal.* **2013,** *298,* 148.

[14] P. Panagiotopoulou, D.I. Kondarides, X.E. Verykios, *Appl. Catal. B* **2009,** *88,* 470.

[15] J. F. Moulder, W. F. Stickle, P. E. Sobol, K. D. Bomben, *Handbook of X-ray Photoelectron Spectroscopy*, (Ed.: J. Chastain) Perkin Elmer Corp., Eden Prairie/USA **1992**.

[16] P.O. Scokart, P.G. Rouxhet, *J. Chem. Soc. Faraday Trans* **1980,** *76,* 1476.

[17] J.C. Lavalley, *Catal. Today* **1996,** *27,* 377.